Magnetic Fields in the 3C 129 Cluster

G. B. Taylor[1], F. Govoni[2], S. W. Allen[3], & A. C. Fabian[3]

ABSTRACT

We present multi-frequency VLA observations of the two radio galaxies 3C 129 and 3C 129.1 embedded in a luminous X-ray cluster. These radio observations reveal a substantial difference in the Faraday Rotation Measures (RMs) toward 3C 129.1 at the cluster center and 3C 129 at the cluster periphery. After deriving the density profile from available X-ray data, we find that the RM structure of both radio galaxies can be fit by a tangled cluster magnetic field with strength 6 μG extending at least 3 core radii (450 kpc) from the cluster center. The magnetic field makes up a small contribution to the total pressure (5%) in the central regions of the cluster. The radio morphology of 3C 129.1 appears disturbed on the southern side, perhaps by the higher pressure environment. In contrast with earlier claims for the presence of a moderately strong cooling flow in the 3C 129 cluster, our analysis of the X-ray data places a limit on the mass deposition rate from any such flow of $<$1.2 $M_{\odot}$ y^{-1}.

Subject headings: galaxies: clusters: individual (3C 129) – intergalactic medium – magnetic fields – polarization – radio continuum: galaxies

1. Introduction

It has been established that radio galaxies embedded in X-ray luminous clusters have high Faraday Rotation Measures (RMs) (*e.g.*, Ge 1991; Taylor, Barton & Ge 1994). Of the 14 cooling flow clusters in the flux limited sample of Edge, Stewart & Fabian (1992) containing a radio source stronger than 100 mJy at 5 GHz, high RMs (greater than 1000 rad m^{-2}) have been found for 9/14 (64%) (Taylor et al. 1994; Taylor et al. 1999). In two with very large cooling flows (PKS 0745$-$191 and A426) no RM can be measured due to a lack of polarized flux. The radio sources in two more clusters are not co-spatial with a cooling flow, and the final source in the sample to be properly studied is the 3C 129 cluster. Furthermore there appears to be a correlation between the cooling flow rate, $\dot{M}$, and the magnitude of the RMs (Taylor et al. 1994). Lower, but significant RMs have

[1]National Radio Astronomy Observatory, Socorro, NM 87801, USA; gtaylor@nrao.edu

[2]Istituto di Radioastronomia del CNR, Via P. Gobetti 101, I-40129 Bologna, Italy; fgovoni@ira.bo.cnr.it

[3]Institute of Astronomy, Madingley Road, Cambridge CB3 0HA, UK; swa@ast.cam.ac.uk;acf@ast.cam.ac.uk

been observed in the A119 cluster (Feretti et al. 1999) which was initially reported to have a weak cooling by Edge et al. (1992), but later found to have no cooling flow (Cirimele, Nesci & Trevese 1997). Some correlation is to be expected since $\dot{M}$ and RM are both related to the central density. The details of this correlation, however, are yet to be understood. In particular we would like to understand how the magnetic fields scale with the density, and if the cooling flow has somehow enhanced the cluster magnetic fields. To this end the study of radio galaxies embedded in clusters both with and without cooling flows is essential.

The RM structure of extended radio galaxies embedded in clusters can provide information about the cluster magnetic fields unavailable by any other means. Besides a measurement of the magnetic field strength (determined in conjunction with X-ray observations of the hot gas), by studying the spatial distribution of the RMs we can estimate the coherence length of the magnetic fields. The RM structure of some cluster radio sources such as Hydra A (Taylor & Perley 1993), Cygnus A (Dreher, Carilli & Perley 1987), and A1795 (Ge & Owen 1993) show ordered structures up to 100 kpc in extent. The origin and evolution of the magnetic fields required to produce such RM structures is a topic of some speculation (Goldman & Rephaeli 1991, DeYoung 1992). They could be remnant magnetic fields of extinct radio galaxies, the result of a cluster dynamo effect (Ruzmaikan et al. 1989), or magnetic fields stripped from spiral galaxies during galactic cannibalism. Cluster magnetic fields are likely to have important effects on cluster dynamics and energy transport (Sarazin 1986; and Tribble 1989), and significant implications for galaxy and cluster formation. By mapping the RM distribution across an embedded source we can measure the correlation length of the cluster magnetic field, and look for sign reversals.

Clusters which contain more than one moderately strong, extended source provide valuable information about the overall extent of the magnetic fields within the cluster. In a recent study of three radio galaxies embedded in the A119 cluster, Feretti et al. (1999), found that the RMs decreased with distance from the cluster center, but were consistent with a magnetic field strength of 10 μG. The 3C 129 cluster is exceptional in that it is one of very few clusters containing two moderately strong ($>$ 100 mJy at 5 GHz) radio sources (see Fig. 1). In fact in the early stages of this project one of us (GBT) failed to appreciate the presence of 3C 129.1 *at the center of the cluster*, so only the RM structure of 3C 129 (which lies 15 arcminutes or a project distance of 400 kpc to the west of the cluster X-ray center) was originally studied.

Observations of both 3C 129 and 3C 129.1 are presented in §2. In §3 we present a detailed multi-frequency, polarimetric study of both 3C 129 and 3C 129.1 including the RM distribution for both radio galaxies. Using these data we attempt in §4 to characterize the magnetic fields (strengths, coherence length, and overall extent) in the 3C 129 cluster.

We assume H_0 = 65 km s^{-1} Mpc^{-1} and q_0=0.5 throughout.

2. Radio Observations and Data Reduction

Observations of both 3C 129 and 3C 129.1 were made at a total of 6 frequencies distributed across the 5 and 8 GHz bands of the VLA (Very Large Array)[4] telescope in 1994 and 2000. The details of the observations are provided in Table 1. The source 3C 138 was used as the primary flux density calibrator, and as an absolute reference for the electric vector polarization angle (EVPA). Phase calibration was derived from the nearby compact source 0420+417 with a cycle time between calibrators of about 12 minutes. Instrumental calibration of the polarization leakage terms was obtained using 0420+417 which was observed over a wide range in parallactic angle. The data were reduced in AIPS (Astronomical Image Processing System), following the standard procedures. The AIPS task IMAGR was used with a suitable taper to make I, Q and U images at each of the 6 frequencies observed at the same resolution. Polarized intensity, P, images and polarization angle, χ, images were derived from the Q and U images. The Faraday Rotation Measure (RM) image was derived from pixel by pixel fits to χ versus λ^2 for all 6 χ images for 3C 129, but the 4.585 GHz data had to be omitted for 3C 129.1 since the polarimetric data at this frequency was corrupted by an incorrect R-L delay setting at the time of observation. Stokes I images using multiple frequencies within an observing band were also produced. In addition to the added sensitivity, the image produced also benefits from improved (u, v) coverage. No correction for the spectral dirty beam has been performed, but the sidelobes expected from this effect should be below the thermal noise floor.

3. X-ray Observations

3.1. ASCA constraints on the X-ray temperature

The 3C 129 cluster was observed with the ASCA satellite on 1998 August 31. For our analysis, we have used the screened event lists available from the Goddard Space Flight Center (GSFC) ASCA archive. The data were reduced using the FTOOLS software (version 4.2) from within the XSELECT environment (version 1.4b). Further data-cleaning procedures including manual screening based on the individual instrument light curves were followed, as recommended in the ASCA Data Reduction Guide (http://legacy.gsfc.nasa.gov/docs/asca/abc/abc.html).

Our primary goal with the ASCA analysis was to obtain a reliable measurement of the mean X-ray gas temperature in the cluster. For this purpose, only data from the two Gas scintillation Imaging Spectrometers (GIS) were used, which had good exposure times of 4.34×10^4 and 4.32×10^4s respectively. Spectra were extracted from circular regions of 9 arcmin radius, centred on the peak of the emission in each detector. Background spectra were determined from the 'blank sky'

[4]The National Radio Astronomy Observatory is a facility of the National Science Foundation operated under cooperative agreement by Associated Universities, Inc.

observations of high Galactic latitude fields compiled during the performance verification stage of the mission. The background data were screened and grade selected in an identical manner to the target observations and the background spectra were extracted from the same regions of the detectors as the target spectra.

The modelling of the ASCA spectra has been carried out using the XSPEC code (version 11.0; Arnaud 1996). Only counts in the energy range $1.5 - 10.0$ keV were used (the energy range over which the calibration of the GIS detectors is currently best understood). The spectra were grouped before fitting to ensure a minimum of 20 counts per PHA channel, thereby allowing χ^2 statistics to be used. The appropriate spectral response matrices, issued by GSFC on 1995 March 6, were used. Auxiliary response files were generated using the ASCAARF software, with effective area calculations appropriate for an extended source.

The spectra have been modelled using the plasma code of Kaastra & Mewe (1993; incorporating the Fe L calculations of Liedhal, Osterheld & Goldstein 1995) and the photoelectric absorption models of Balucinska-Church & McCammon (1992). The data for both GIS detectors were analysed simultaneously, using a model appropriate for an isothermal plasma in collisional equilibrium at the optically-determined redshift for the cluster, absorbed by an equivalent hydrogen column density, $N_{\rm H}$ of solar metallicity cold gas. The temperature (kT), metallicity (Z) and absorbing column density were linked to take the same values across the two GIS data sets, although the normalizations were allowed to vary as independent fit parameters. We find that this model provides an acceptable description of the ASCA data with $\chi^2 = 995$ for 1012 degrees of freedom and best-fit parameter values $kT = 6.25^{+0.27}_{-0.26}$ keV, $Z = 0.31 \pm 0.03$ solar and $N_{\rm H} = 6.41 \pm 0.44 \times 10^{21}$ atom cm^{-2} (90 per cent confidence limits).

The mean X-ray gas temperature measured within the central 9 arcmin radius with ASCA is consistent with the value of $5.6^{+0.7}_{-0.6}$ keV determined by Edge & Stewart (1991) using EXOSAT Medium Energy Proportional Counter Array observations (which covered a larger 45×45 arcmin^2 field of view). Our ASCA result is slightly hotter than the value of 5.5 ± 0.2 keV measured by Leahy & Yin (2000) from a joint analysis of the same EXOSAT data and a short (500s) ROSAT Position Sensitive Proportional Counter observation. The absorbing column density measured with ASCA is in good agreement with the Galactic value along the line of sight to the cluster of 7.1×10^{21} atom cm^{-2} (Dickey & Lockman 1990) or 5.8×10^{21} atom cm^{-2} (Stark et al. 1992).

3.2. The X-ray gas density profile

Pointed X-ray imaging observations of the 3C 129 cluster have been made with the High Resolution Imager (HRI) and Imaging Proportional Counter (IPC) on the Einstein Observatory and the HRI on ROSAT. The observation best suited to the current task of measuring the X-ray gas density profile in the regions surrounding the 3C 129 and 3C 129.1 radio galaxies is the Einstein IPC observation, which was made on 1980 October 4. For our analysis, we have used the processed

0.2 – 3.5 keV image available from the GSFC on-line archive. The net exposure time for the IPC observation is 6847s.

In order to determine the X-ray gas density profile and to discriminate on the presence/absence of any cooling flow in the cluster core, we have carried out a deprojection analysis of the Einstein IPC image using an updated version of the deprojection code of Fabian et al. (1981; see also White, Jones & Forman 1997 for details). An azimuthally-averaged X-ray surface brightness profile was constructed from the IPC image, with a radial bin-size of 0.8 arcmin (23 kpc). This profile is used as the primary input for the deprojection analysis. The deprojection method also requires the total mass profile for the cluster to be specified. We have iteratively determined the mass profile (parameterized using the formalism of Navarro, Frenk & White 1997) that results in a deprojected temperature profile that is approximately isothermal, within the regions probed by the IPC data, and is consistent with the mean gas temperature determined from the ASCA data.[5]

The electron density profile for the central 600 kpc ($\sim$ 21 arcmin) radius region, determined from the deprojection analysis, is shown in Fig. 2. The best-fitting $\beta-$model (overlaid) has parameter values $r_{\rm c} = 146 \pm 26$ kpc, $\beta = 0.47 \pm 0.05$ and $n_{\rm e}(0) = 2.8 \pm 0.3 \times 10^{-3}$ cm^{-3}. We note, however, that the $\beta-$model provides a poor fit to the data, with a reduced χ^2 value $\sim$ 3.6. The formal errors on the best-fit parameter values ($\Delta\chi^2 = 2.7$ limits) are therefore likely to underestimate the true uncertainties. Our results on the density profile are in good agreement with those presented by Leahy & Yin (2000).

The central cooling time in the cluster (the mean cooling time within the central 0.8 arcmin bin) is $t_{\rm cool} = 1.32^{+0.66}_{-0.36} \times 10^{10}$ yr. We determine a 90 per cent confidence upper limit on the cooling radius (at which the cooling time first exceeds a Hubble time) of $r_{\rm cool} < 34$ kpc, and a limit on the mass deposition rate within this radius of < 1.2 M$_\odot$ y^{-1}. These results are consistent with the previous findings of White et al. (1997) and show that the 3C 129 cluster does not contain a strong cooling flow. They are inconsistent with the results of Leahy & Yin (2000) who claim a cooling flow of 84 M$_\odot$ y^{-1} based on the excess luminosity over their β-profile fit.

4. Results

We present multifrequency radio observations, polarization properties, and rotation measure distributions for 3C 129 and 3C 129.1. Properties derived for both sources are summarized in Table 2.

[5]The best-fit parameterized mass model has a scale radius $r_s \sim 0.8$ Mpc, a concentration parameter $c \sim 2.7$ and an equivalent velocity dispersion $\sigma = \sqrt{50} H_0 r_s c \sim 1000$ km s^{-1}.

4.1. 3C 129, Cluster Periphery

The radio source 3C 129 was identified with an E galaxy by Hill & Longair (1971), and was among the first radio galaxies discovered to have a head-tail structure. Since then it has been studied extensively in the radio by several authors (e.g., Miley 1973, Perley & Erickson 1979, van Breugel 1982, Downes 1984, Feretti et al. 1998). Low frequency observations by van Breugel & Jägers (1982) show that the radio tail extends over $\sim 20'$ in length (> 0.5 Mpc), making 3C 129 sometimes classified as one of the giant radio galaxies (Ishwara-Chandra & Saikia 1999). Our relatively high frequency interferometry observations are only sensitive to the brighter emission from the inner $2'$ or "head" of 3C 129.

The jets in 3C 129 start out oppositely directed nearly north-south and then curve continuously to the northwest. The more prominent, northern jet expands gradually, while the southern jet flares more abruptly where it makes a sharp bend about $30''$ west of the nucleus. At large distances from the nucleus the lobes merge together and bend to the west and southwest. We measure an integrated flux density of 1300 mJy (49%) out of the total flux density of 2650 mJy measured with the Effelsberg 100 m antenna (Feretti et al. 1998). Our images agree with, but have greater sensitivity than the early 5 GHz VLA images presented by Rudnick & Burns (1981).

At 8.5 GHz the polarized intensity in the jets is around 10% and increases to 20-30% in the lobes. The core is less than 0.5% polarized. Similar values are seen at 5 GHz, except in some filamentry regions of very low polarization running across the lobes. A plot of the polarized intensity and magnetic field vectors (corrected for the effects of RM) is shown in Fig. 3.

Early Faraday Rotation Measure (RM) estimates for 3C 129 were -30 rad m^{-2}(van Breugel 1982), but further observations by Downes (1984) demonstrated that the early observation suffered from an $n\pi$ ambiguity and the correct value (at $4.3'$ resolution) was -130 ± 5 rad m^{-2}. At high resolution ($1.8''$) we find the RMs in 3C 129 range from -400 to 100 rad m^{-2} (see Fig. 4), but cluster around the average value of -125 rad m^{-2}, with a dispersion of 82 rad m^{-2}. The error in the determination of the RM varies with SNR across each source, but is generally less than 20 rad m^{-2}(1σ). Downes (1984) also found that the fractional polarization continues to increase along the tails to a peak of about 50% at $10'$ from the nucleus while the integrated RM stays constant. These RMs are somewhat larger than expected for a typical field galaxy along this line-of-sight which are in the range -40 to 40 rad m^{-2} (Simard-Normandin, Kronberg & Button 1981), but substantially lower than are found for 3C 129.1 at the cluster center. The RMs in Fig. 4 are patchy with a scale of $\sim$5–10 kpc. No apparent correlation of the RMs with total or polarized intensity is seen.

4.2. 3C 129.1, Cluster Center

The radio galaxy 3C 129.1 is usually mentioned in passing in papers concentrating on its larger and brighter cousin. In early papers its proximity and similar redshift to 3C 129 was taken as indicative of clustering, although the low galactic latitude made optical identification of other cluster members difficult. The discovery of strong and extended X-ray emission by the *Uhuru* satellite confirmed that both radio galaxies are indeed members of a cluster.

The radio source 3C 129.1 is an order of magnitude more compact (about $1.5'$) than 3C 129 (see Fig. 1). The morphology is similar to most FR I radio galaxies, with bright regions on either side of the core that fade with distance from the core, but on the southwest side there is a sharp boundary to the radio emission that is uncharacteristic of FR Is.

At both 5 and 8 GHz, the bright inner $30''$ are polarized at the level of 10%. The fractional polarization increases to 20-30% in the fainter outer regions. The core has less than 2% polarization. A plot of the polarized intensity and magnetic field vector orientation is shown in Fig. 5. Examination of polarimetry from the NVSS at 1.4 GHz (Condon et al. 1998) shows between 0.2 and 1% polarization in 3C 129.1 compared to 1 – 40% in 3C 129 – consistent with the depolarizing effects of high RMs towards 3C 129.1.

The RMs in 3C 129.1 are shown in Fig. 6 and range from -600 to $+750$ rad m^{-2}, considerably larger than those in 3C 129. Histograms of the RM distributions for both sources (Figures 7 and 8) illustrate the differences in both the average and the dispersion of the RM between these two sources. The error in the determination of the RM varies with SNR across each source, but is generally less than 20 rad m$^{-2}(1\sigma)$. The scale size of the RMs in 3C 129.1 appears smaller, $\sim$3 kpc. Over most of the sources the RMs trend up or down smoothly, but there are a few sign reversals between adjacent patches.

5. Discussion

5.1. Radio Source Properties

The head-tail radio sources like 3C 129 are usually found at the periphery of clusters. The usual explanation for this morphology is that the jets are swept back by relative motion between the radio galaxy and the IGM. Rudnick & Burns (1981) estimated a relative velocity between 3C 129 and the IGM of 3000 km s^{-1} using a cluster gas density of $\sim$$10^{-4}$ cm^{-3}. This is comparable to the density derived from the X-ray observations in §3.2 of 6×10^{-4} cm^{-3}.

The compactness of 3C 129.1 is probably a direct result of its central location within the cluster. This is similar, but less extreme than the distortions seen in the radio emission from the cD galaxies PKS 0745−191 (Taylor, Barton & Ge 1994) and 3C 317 (Zhao et al. 1993).

5.2. The Galactic RM Contribution

At the low galactic latitude of the 3C 129 cluster (l,b = 160.4, 0.1°), the galactic RM contribution could be substantial. This contribution may be in the form of (1) an additive offset to the RMs, and (2) point-to-point variations in the RM distribution. In regards to point (1) the constant RM of -130 rad m^{-2} over $10'$ (12 pc at a distance of 4 kpc, 250 kpc at the distance of 3C 129) found by Downes (1984) is more readily explained as the result of a Galactic offset rather than a cluster magnetic field organized over such a large scale. Regarding point (2) above, Clegg et al. (1992) have examined the RMs of extragalactic sources between galactic longitudes of 30 and 90 degrees in order to examine the magnetoionic structure of the Galaxy. For sources at low galactic latitudes ($|b| < 5°$) with two or more components seperated by less than 1° they find RM differences up to 180 rad m^{-2}, although typical values are more like 50 rad m^{-2}. In 3C 129 the RM difference between adjacent regions in the radio lobes ranges up to 400 rad m^{-2}. Unless the Galaxy has an exceptionally strong and tangled magnetoionic structure at $l = 160°$, our observations of 3C 129 are difficult to explain entirely by a galactic RM. For several radio galaxies within 10 degrees of the 3C 129 cluster (including 3C 134 at $l, b = 168, -1.9°$) Simard-Normandin et al. (1981) find RMs in the range -40 to 40 rad m^{-2}, indicating that the galactic field strengths are not particularly large in this direction. The nearly factor 3 larger RM dispersion in 3C 129.1 would be even more difficult to explain as a galactic effect. For the remainder of this paper we consider the 3C 129 cluster to be the dominant contributor to the RM variations seen across both 3C 129 and 3C 129.1. This interpretation is consistent with the accumulating evidence for cluster magnetic fields (discussed in §1) and the large contrast in RM distribution between 3C 129.1 at the cluster center and 3C 129 at the periphery.

5.3. Cluster Magnetic Field Strengths and Topologies

For Faraday rotation from a magnetized cluster gas, the RMs are related to the density, $n_{\rm e}$, and magnetic field along the line-of-sight, $B_{||}$, through the cluster according to

$$RM = 812 \int_0^L n_{\rm e} B_{||} {\rm d}l \text{ rad m}^{-2} , \tag{1}$$

where $B_{||}$ is measured in μGauss, $n_{\rm e}$ in cm^{-3} and dl in kpc. If the density distribution and magnetic field topology are known then it is possible to solve for the magnetic field strength.

The simplest case is that of a constant density and uniform magnetic field out to some distance from the cluster center. If we consider the maximum RM from 3C129.1 at the center of 600 rad m^{-2}, then using the central density and core radius derived in §3.2, the magnetic field needed to produce this RM is 1.8 μG. This field can be thought of as a lower limit to the true field strength since any reversals of the magnetic field would require a larger field strength to produce the observed

RM. Such field reversals are certainly present as the patchy RM distribution in 3C 129.1 (Fig. 6) clearly indicates.

A more reasonable field topology is that of cells of constant size, density, and magnetic field strength, but a random magnetic field direction, uniformly filling the entire cluster. The Faraday RM produced by such a screen will be built up in a random walk fashion and will thus have an average value of 0 rad m^{-2}, but a dispersion in the RM, σ_{RM}, that is proportional to the square root of the number of cells along the line-of-sight through the cluster. For a density distribution that follows a β-profile, Felten (1996) has derived the following relation for the RM dispersion:

$$\sigma_{\mathrm{RM}} = \frac{\mathrm{K}B\ n_0\ r_c^{1/2} l^{1/2}}{(1 + r^2/r_c^2)^{(6\beta-1)/4}} \sqrt{\frac{\Gamma(3\beta - 0.5)}{\Gamma(3\beta)}} \tag{2}$$

where n_0, r_c, and β are derived in §3.2, l is the cell size, r is the distance of the radio source from the cluster center, Γ is the Gamma function, and K is a factor which depends on the location of the radio source along the line-of-sight through the cluster: K = 624 if the source is beyond the cluster, and K = 441 if the source is halfway through the cluster. We assume that both 3C 129 and 3C 129.1 are embedded halfway through the cluster. This is a good assumption for 3C 129.1 at the center of the cluster, but could be considerably off for 3C 129 at the periphery. For the field size, l, we use the scale size of 5 kpc seen in the RM distributions. With the above measurements or assumed values, we use the estimated RM dispersion (Figs. 9 and 10) for 3C 129 and 3C 129.1 to estimate the cluster magnetic field strength at 6.1 and 5.6 μG respectively. The good agreement between the field strengths estimated from these two sources is encouraging, although this model is probably still too simple to hold up to more rigorous tests. Probably both l and B change with distance from the cluster center, and the density distribution may be considerably more complex, especially at the center of the cluster and in the vicinity of a powerful radio galaxy.

The estimated cluster magnetic field strength of 6 μG compares favorably to the magnetic field strength of 5–10 μG found in A119 by Feretti et al. (1999) through a similar analysis of 3 embedded radio galaxies. These field strengths are somewhat less than the $\sim$30 μG derived for sources embedded in strong cooling flows like Hydra A (Taylor & Perley 1993). The magnetic field pressure in the 3C 129 cluster corresponds to 5% of the combined magnetic and thermal gas pressure at the cluster center. At the projected distance of 3C 129 of 400 kpc, this simple model for the magnetic field predicts nearly a fifth of the combined pressure comes from the magnetic fields.

Based on the data presented here we cannot rule out the possibility that the cluster gas density and magnetic fields are enhanced in the vicinity of the radio sources and that this "cocoon" provides the observed Faraday screen. However, the recent demonstration of a RM excess towards *background* radio sources seen through clusters by Clarke, Kronberg & Böhringer (2001) argues convincingly in favor of cluster-wide magnetic fields.

6. Conclusions

The 3C 129 cluster is exceptional in that it possesses two bright, extended radio galaxies embedded in a hot X-ray emitting gas. We have reanalyzed available X-ray data to determine the density profile and combined this information with high resolution radio measurements of the Faraday Rotation Measure structure to provide information on the magnetic field strengths and topologies. The Faraday Rotation Measure images reveal a patchy structure with a scale length of $\sim$5 kpc indicating that the magnetic fields are tangled on this scale. A simple model with a magnetic field in randomly oriented cells of uniform size and strength, and a gas density distribution given by a β profile, yields a magnetic field strength of $\sim$6 μG out to $\sim$450 kpc. These magnetic fields will have a significant impact on energy transport through the cluster, and may be dynamically important as well. Although our reanalysis of the X-ray data does not reveal the cooling flow suggested in the past (Edge et al. 1992; Leahy & Yin 2000), the field strengths derived are similar to those found in cooling flow clusters. This supports claims by Feretti et al. (1999) and Clarke, Kronberg & Böhringer (2001) that magnetic fields are pervasive in galaxy clusters.

We also find that the deeply embedded radio galaxy 3C 129.1 appears more strongly confined on the southern side. Higher resolution X-ray observations with Chandra will reveal if the thermal gas pressure is enhanced in this region.

Future observations with an Expanded Very Large Array (EVLA) could increase the number of radio galaxies for which we can image the rotation measure distribution tenfold. This would provide many more constraints on the magnetic field topology in clusters.

SWA and ACF acknowledge the support of the Royal Society. This research has made use of the NASA/IPAC Extragalactic Database (NED) which is operated by the Jet Propulsion Laboratory, Caltech, under contract with NASA.

REFERENCES

Arnaud, K.A. 1996, in "Astronomical Data Analysis Software and Systems V", eds. Jacoby, G. & Barnes, J., ASP Conf. Series Vol. 101, p. 17

Balucinska-Church, M.,& McCammon, D. 1992, ApJ, 400, 699

van Breugel, W. J. M. 1982, A&A, 110, 225

van Breugel, W. J. M., & Jägers, W. J. 1982, A&AS, 49, 529

Clarke, T. E., Kronberg, P. P., & Böhringer, H. 2001, ApJ, 547, L111

Clegg, A. W., Cordes, J. M., Simonetti, J. M., & Kularni, S. R. 1992, ApJ, 386, 143

Condon, J. J., Cotton, W. D., Greisen, E. W., Yin, Q. F., Perley, R. A., Taylor, G. B. & Broderick, J. J. 1998, AJ, 115, 1693

Cirimele, G., Nesci, R., & Trevese, D. 1997, ApJ, 475, 11

DeYoung, D. S. 1992, ApJ, 386, 464

Dickey J. M., & Lockman F. J. 1990, ARA&A, 28, 215

Downes, A. 1984, MNRAS, 211, 215

Dreher, J. W., Carilli, C. L., & Perley, R. A. 1987, ApJ, 316, 611

Edge, A. C., & Stewart, G. C. 1991, MNRAS, 252, 414

Edge, A. C., Stewart, G. C., & Fabian, A. C. 1992, MNRAS, 258, 177

Fabian, A. C., Hu, E. M., Cowie, L. L., & Grindlay, J. 1981, ApJ, 248, 47

Felten, J. B. 1996, in "Clusters, Lensing and the Future of the Universe" eds. Trimble, V., & Reisenegger, A., ASP Conf. Series, Vol. 88, p. 271

Feretti, L., Giovannini, G., Klein, U., Mack, K.-H., Sijbring, L. G., & Zech, G. 1998, A&A, 331, 475

Feretti, L., Dallacasa, D., Govoni, F., Giovannini, G., Taylor, G. B., & Klein, U. 1999, A&A, 344, 472

Goldman, I., & Rephaeli, Y. 1991, ApJ, 380, 344

Ge, J.-P. 1991, Ph.D. thesis, New Mexico Institute of Mining and Technology

Ge, J.-P., & Owen, F. N. 1993, AJ, 105, 778

Hill, J. M., & Longair, M. S. 1971, MNRAS, 154, 125

Ishwara-Chandra, C. H., & Saikia, D. J. 1999, MNRAS, 309, 100

Kaastra, J. S., & Mewe, R. 1993, Legacy, 3, HEASARC, NASA

Leahy, D. A., & Yin, D. 2000, MNRAS, 313, 617

Liedhal, D. A., Osterheld, A. L., & Goldstein, W. H. 1995, ApJ, 438, L115

Miley, G. K. 1973, A&A, 26, 413

Navarro, J. F., Frenk, C. S., & White, S. D. M. 1997, ApJ, 490, 493

Perley, R. A., & Erickson, W. C. 1979, ApJS, 41, 131

Rudnick, L., & Burns, J. O. 1981, ApJ, 246, L69

Ruzmaikan, A. A., Sokoloff, D. D., & Shukurov, A. 1989, MNRAS, 241, 1

Sarazin, C. L. 1986, Rev. Mod. Phys., 58, 1

Simard-Normandin, M., Kronberg, P. P., & Button, S. 1981, ApJS, 45, 97

Stark, A. A. et al. 1992, ApJS, 79, 77

Taylor, G. B. & Perley, R. A. 1993, ApJ, 416, 554

Taylor, G. B., Barton, E. J., & Ge, J.-P. 1994, AJ, 107, 1942.

Taylor, G. B., Allen, S. W., & Fabian, A. C. 1999 in "Diffuse Thermal and Relativistic Plasma in Galaxy Clusters" eds. Bohringer, H., Feretti, L., & Schuecker, P., MPE Report No. 271, p. 77.

Tribble, P. C. 1989, MNRAS, 238, 1247

White, D. A., Jones, C., & Forman, W. 1997, MNRAS, 292, 419

Zhao, J.-H., Sumi, D. M., Burns, J. O., & Duric. N. 1993, ApJ, 416, 51

This preprint was prepared with the AAS LaTeX macros v5.0.

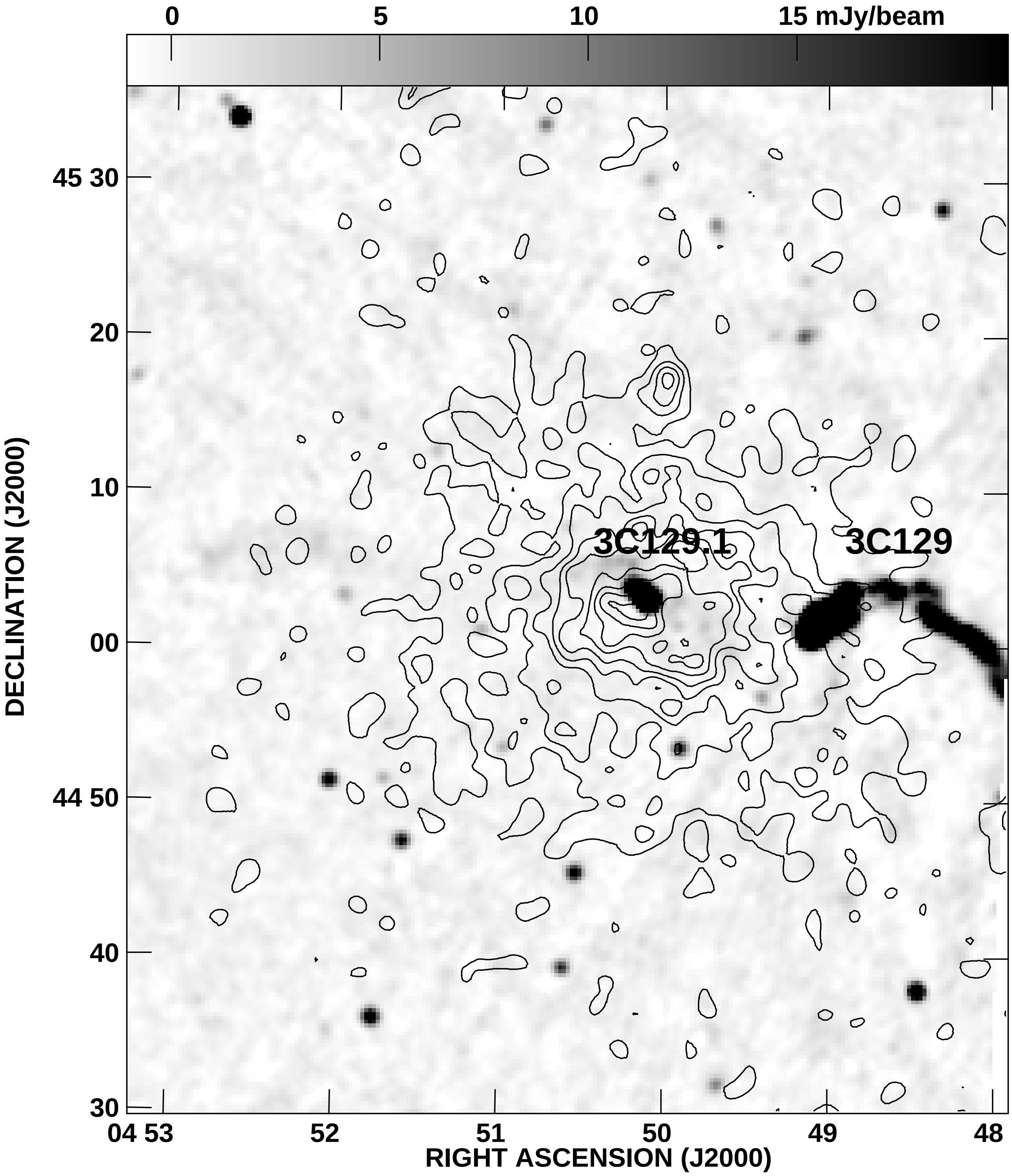

Fig. 1.— The 3C 129 cluster in the X-ray (contours from the Einstein IPC image) and radio (greyscale from the NVSS, with range −1 to 20 mJy/beam.). The resolution is roughly 45″ in both images.

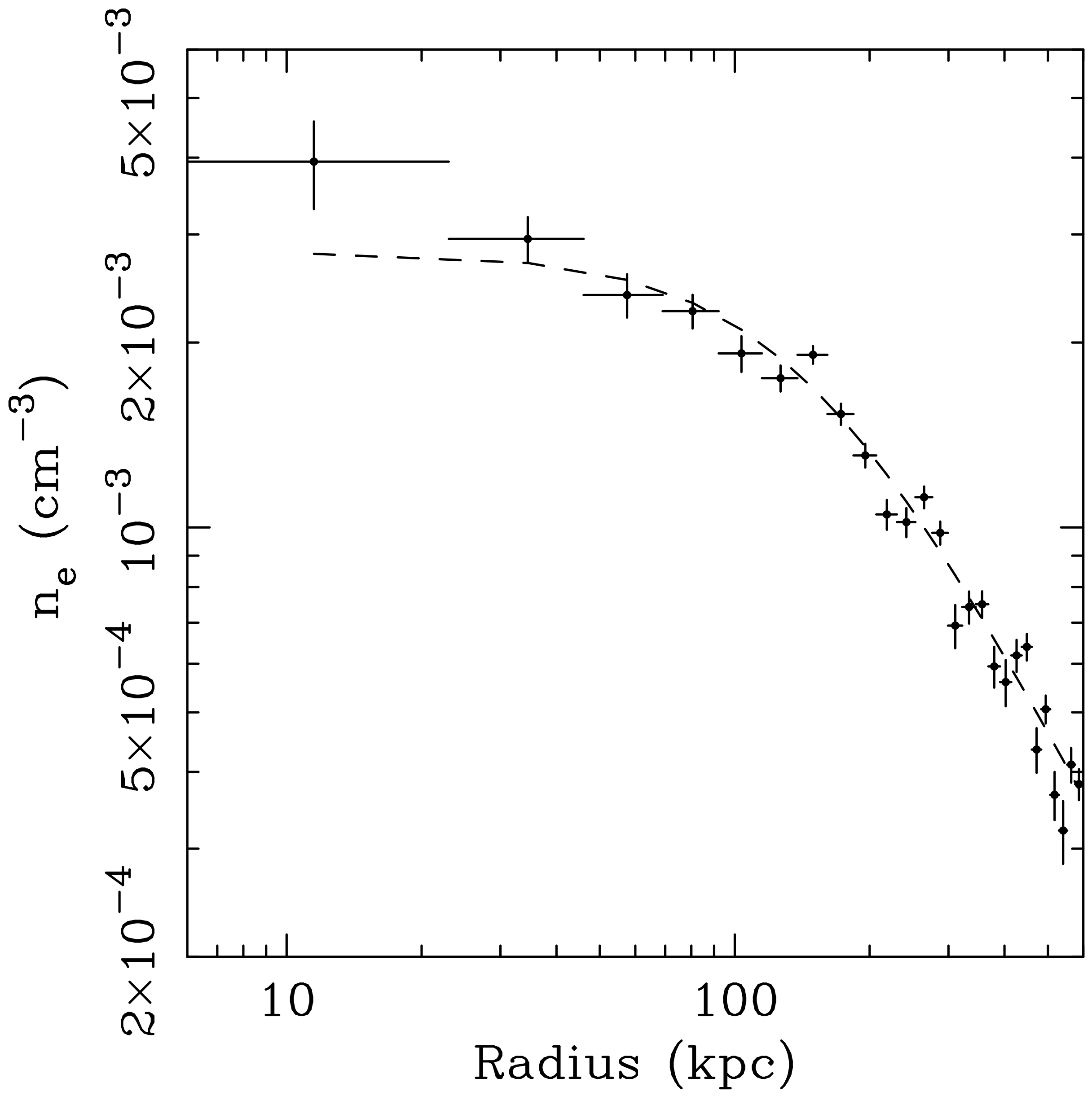

Fig. 2.— The electron density profile determined from the deprojection analysis of the Einstein IPC X-ray image. Error bars are 1σ uncertainties determined from 100 Monte Carlo simulations. A mean gas temperature of 6.25 keV, an absorbing column density of 6.4×10^{21} atom cm^{-2} and a metallicity of 0.31 solar are assumed (in agreement with the results determined from the ASCA spectra).

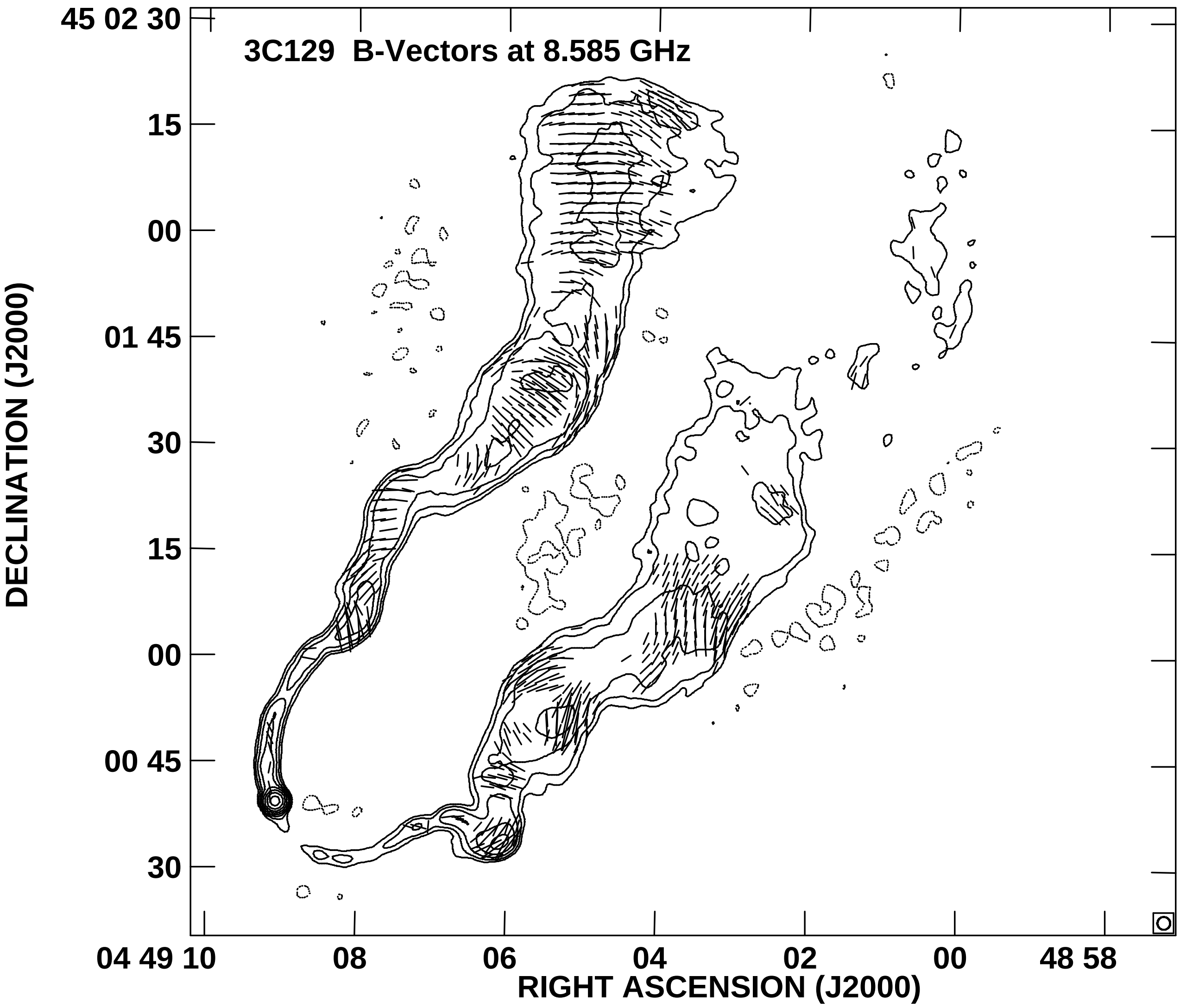

Fig. 3.— Polarized intensity projected magnetic field vectors at 8.6 GHz (1 arcsec = 0.14 mJy/beam; vectors corrected for Faraday rotation) overlaid on total intensity contours for 3C 129. Contours start at 0.2 mJy/beam and increase by factors of 2. The peak in the image is 37 mJy/beam. The restoring beam is plotted in the lower right corner and is a circular Gaussian with a FWHM of 1.8 arcseconds.

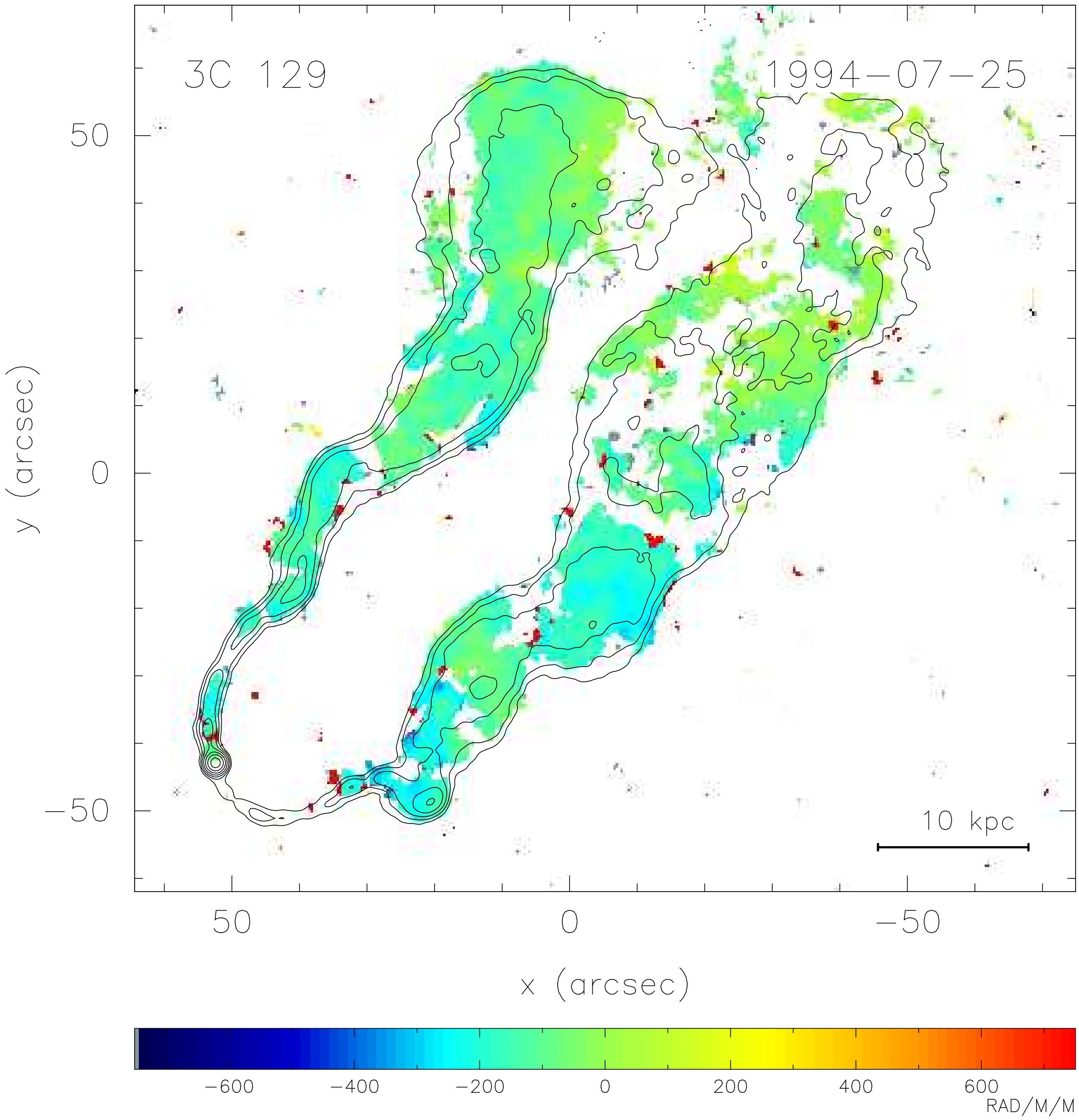

Fig. 4.— Rotation measure image of 3C 129 with contours of total intensity at 4.7 GHz overlaid. The colorbar ranges from -750 to $+750$ rad m^{-2}. Due to the low blanking level chosen in order to see the RMs in the faint lobes, some spurious RMs show up as red or black spots at the edges (or beyond) regions of polarized emission.

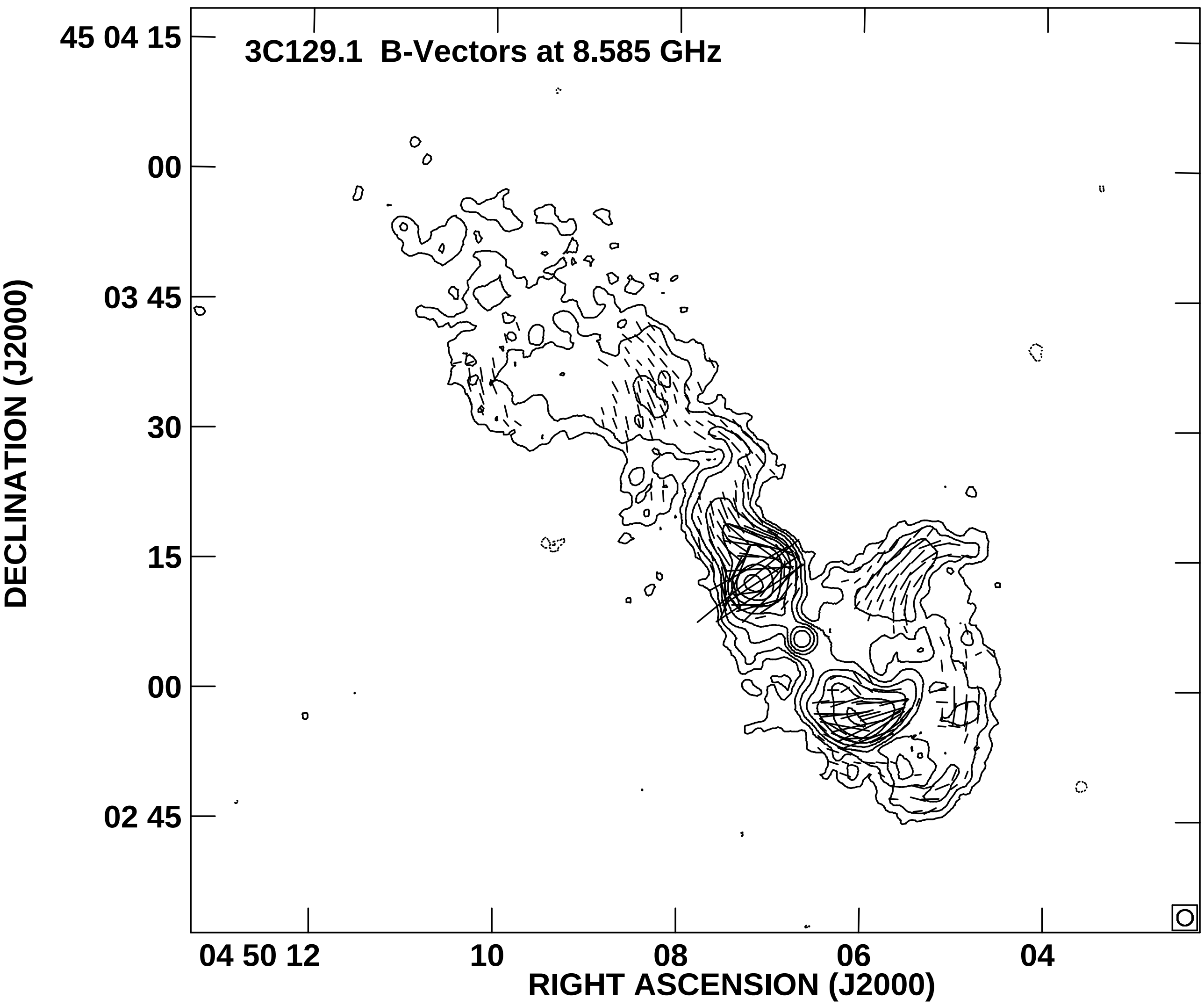

Fig. 5.— Polarized intensity projected magnetic field vectors at 8.6 GHz (1 arcsec = 0.071 mJy/beam; vectors corrected for Faraday rotation) overlaid on total intensity contours for 3C 129.1. Contours start at 0.05 mJy/beam and increase by factors of 2. The peak in the image is 7.9 mJy/beam. The restoring beam is plotted in the lower right corner and is a circular Gaussian with a FWHM of 1.8 arcseconds.

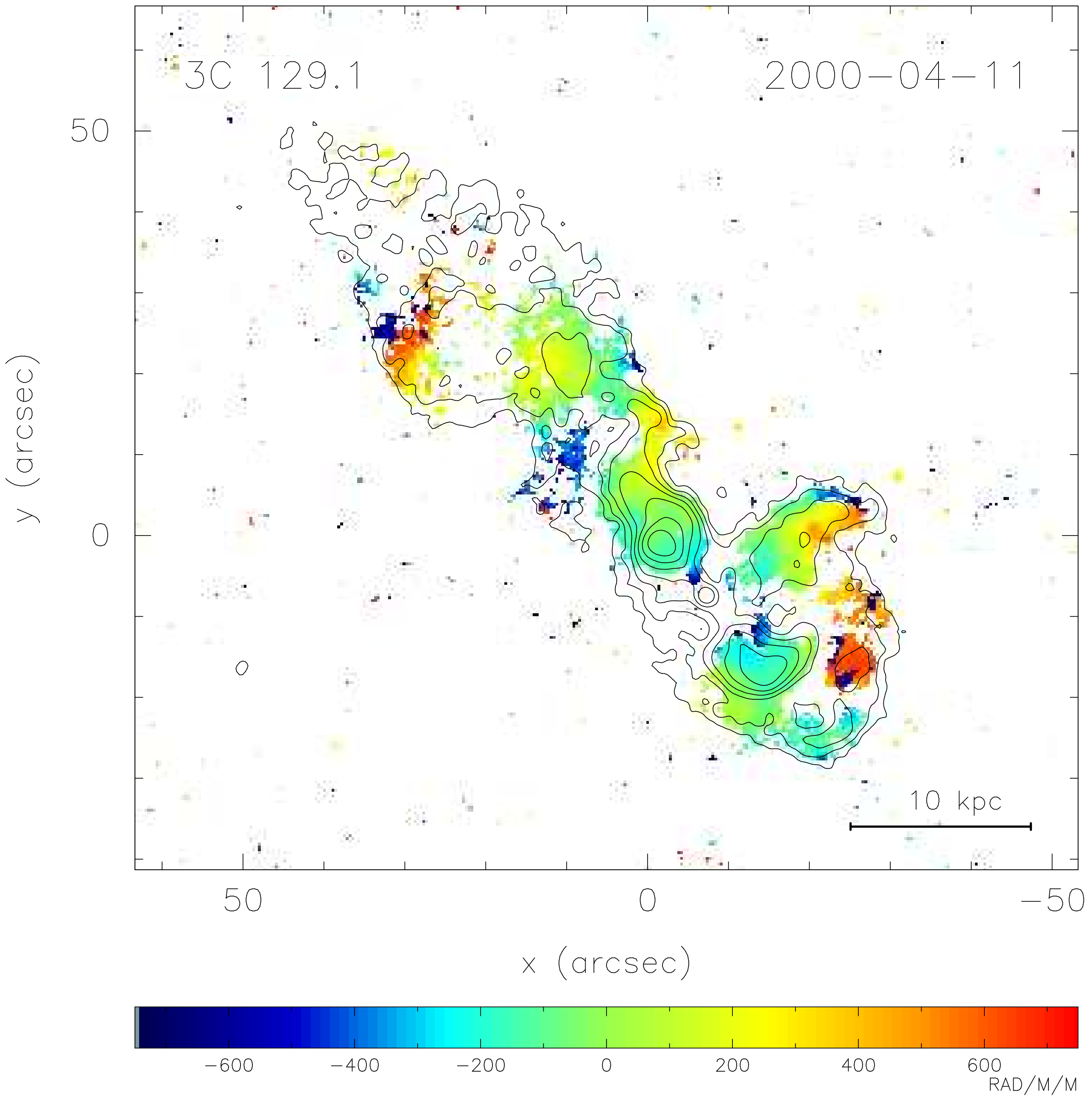

Fig. 6.— Rotation measure image of 3C 129.1 with contours of total intensity at 4.9 GHz overlaid. The colorbar ranges from −750 to +750 rad m^{-2}.

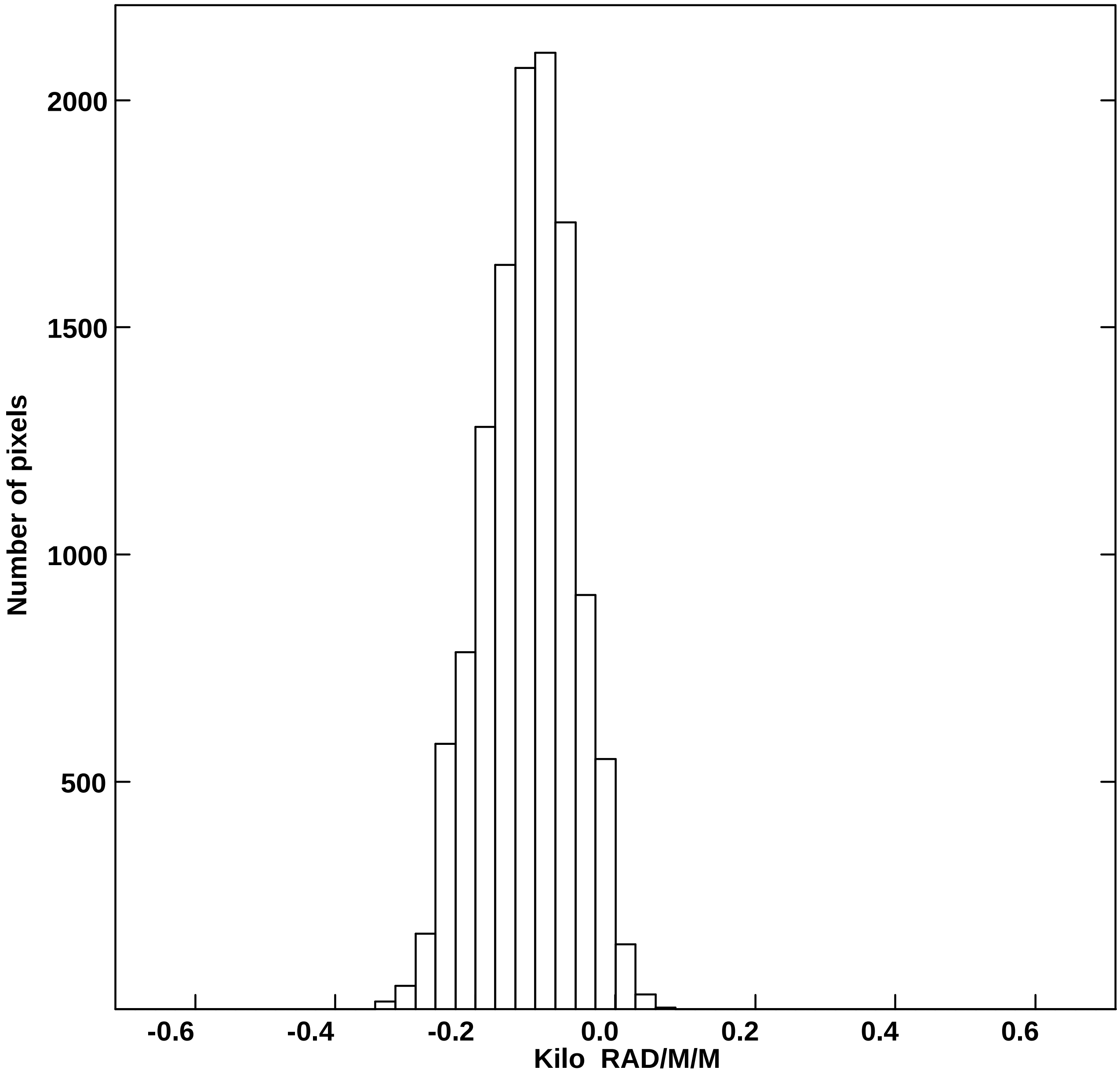

Fig. 7.— Rotation measure distribution for 3C 129. The mean value is -125 rad m^{-2} with dispersion of 82 rad m^{-2}.

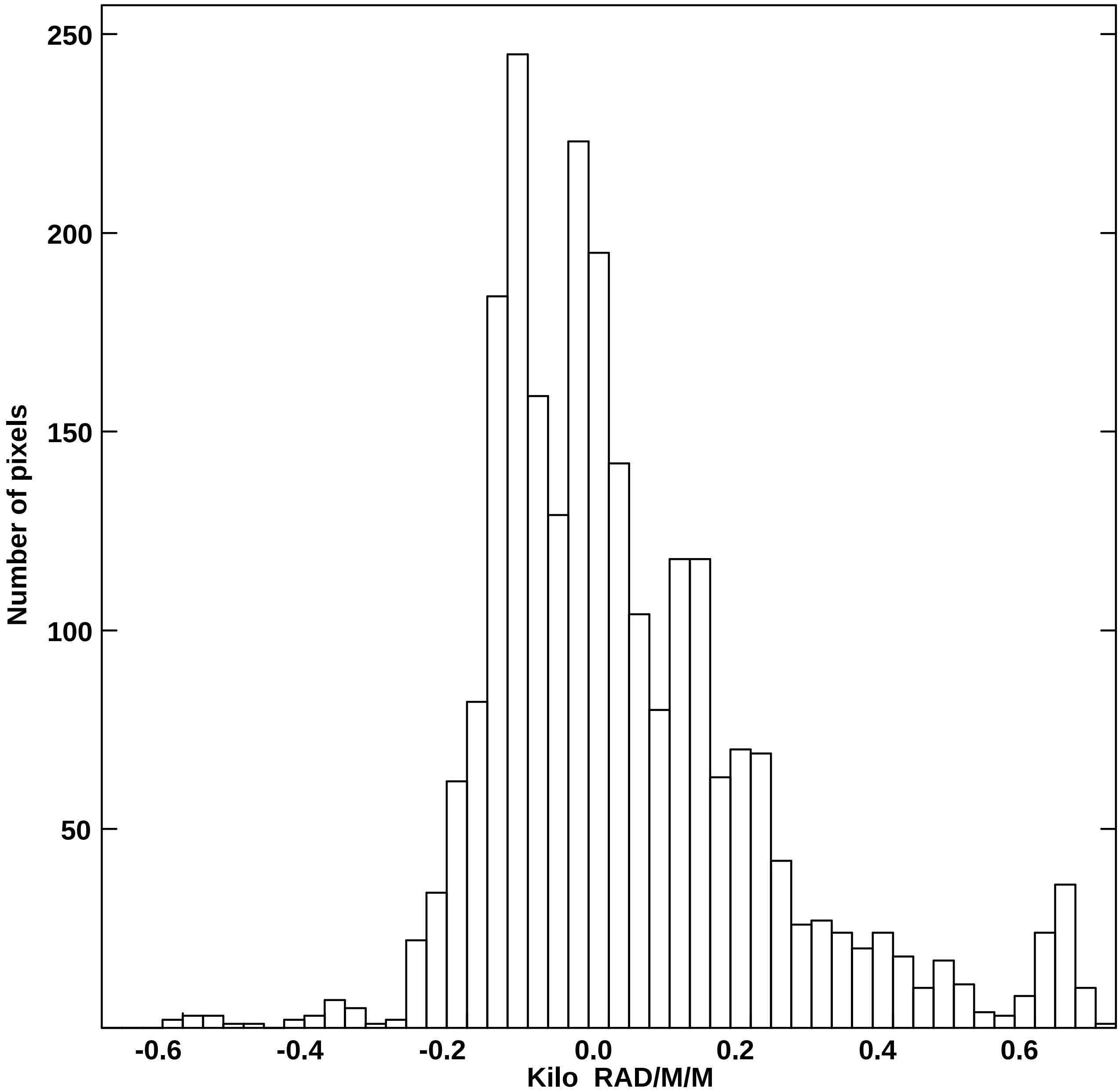

Fig. 8.— Rotation measure distribution for 3C 129.1. The mean value is 21 rad m^{-2} with dispersion of 200 rad m^{-2}.

TABLE 1

OBSERVATIONAL PARAMETERS

Source	Date	Frequency (MHz)	Bandwidth[a] (MHz)	Config.	Duration (hours)
3C 129	Jul1994	4585/4885	50	B	1.09
	Jul1994	7815/8165	50	B	1.06
	Jul1994	8515/8885	50	B	1.08
	Nov1994	4585/4885	50	C	0.21
	Nov1994	7815/8165	50	C	0.64
	Nov1994	8515/8885	50	C	0.60
3C 129.1	Feb2000	4585[a]/4885	50	B	1.75
	Feb2000	7815/8165	50	B	1.69
	Feb2000	8515/8885	50	B	1.79
	Apr2000	4585[a]/4885	50	C	0.72
	Apr2000	7815/8165	50	C	0.90
	Apr2000	8515/8885	50	C	0.77

[a] Due to an incorrect delay setting for the BD IF pair in the 5 GHz (6 cm) band, the 4585 MHz polarimetry from the Feb2000 and Apr2000 runs were rendered unusable.

TABLE 2

SOURCE PROPERTIES

Property	3C 129	3C 129.1
core RA (J2000)	$04^h49^m09\overset{s}{.}0760$	$04^h50^m06\overset{s}{.}6308$
Dec. (J2000)	$45°00'39\overset{''}{.}215$	$45°03'05\overset{''}{.}990$
radial velocity	6240 km s^{-1}	6675 km s^{-1}
projected distance	0.4 Mpc	0 Mpc
angular size	$20'$	$1.5'$
physical size	500 kpc	40 kpc
flux density (5 GHz)	2650[a] mJy	220 mJy
power (5 GHz)	2.96×10^{24} W Hz^{-1}	0.25×10^{24} W Hz^{-1}
<RM>	−125 rad m^{-2}	21 rad m^{-2}
σ_{RM}	82 rad m^{-2}	200 rad m^{-2}
$\|RM_{max}\|$	260 rad m^{-2}	640 rad m^{-2}

[a] Based on observations by Feretti et al. (1998) with the Effelsberg 100 m antenna.